

## 13. Materials Considerations and Data Base

### 13.1 Introduction

A wide range of structural materials was originally considered for the APEX project. This list included conventional materials (e.g., austenitic stainless steel), low-activation structural materials (ferritic-martensitic steel, V-4Cr-4Ti, and SiC/SiC composites), oxide dispersion strengthened ferritic steel, conventional high temperature refractory alloys (Nb, Ta, Mo, W alloys), Ni-based super alloys, ordered intermetallics (TiAl, Fe<sub>3</sub>Al, etc.), various composite materials (C/C, Cu-graphite and other metal-matrix composites, Ti<sub>3</sub>SiC<sub>2</sub>, etc.), and porous-matrix metals and ceramics (foams). In order to provide maximum flexibility in the design (and to increase the possibility for significant improvements in reactor power density), low long-term activation was not used as a defining “litmus test” for the selection of candidate materials.

Due to limitations in resources and time, the materials analysis for APEX quickly focused on refractory alloys due to their higher thermal stress capacity and higher operating temperature capabilities compared to conventional structural materials (see below). However, it should be emphasized that conventional materials may work satisfactorily in some of the APEX concepts (e.g., austenitic stainless steel located behind a thick wall of Flibe). Other promising advanced structural materials (e.g., ODS alloys, intermetallics) should be considered in future analyses.

Numerous factors must be considered in the selection of structural materials, including

- unirradiated mechanical and thermophysical properties
- chemical compatibility and corrosion
- material availability, cost, fabricability, joining technology
- radiation effects (degradation of properties)
- Safety and waste disposal aspects (decay heat, etc.)

Information assembled by the APEX team during past 18 months on the first four items in this list is summarized in this chapter.

#### 13.1.1 Material costs and fabrication issues

The APEX materials team gathered information on the costs of many of the candidate structural materials. This raw material cost information is summarized in Table 13.1. The fabrication costs for producing finished products of refractory alloys (particularly W) is known to be much higher than for steels. The Group V refractory metals (V, Nb, Ta) are relatively easy to fabricate into various shapes such as tubing, whereas the Group VI refractory metals (Mo, W) are very difficult to fabricate. A further issue with all of the refractory metals is joining, particularly in-field repairs. Satisfactory full-penetration welds have not been developed for W, despite intensive efforts over a >25 year time span (1960-1985). The main issue associated with fusion zone welding of the Group V alloys is the pickup of embrittling interstitial impurities (O, C, N, H) from the atmosphere. Work is in progress to develop satisfactory fusion welds for vanadium alloys. One promising alternative joining technique that has recently been developed by the aerospace industry is stir friction welding.

Table 13.1 Costs for simple plate products (1996 prices)

Material	Cost per kg
Fe-9Cr steels	≤\$5.50 (plate form)
SiC/SiC composites	>\$1000 (CVI processing) ~\$200 (CVR processing of CFCs)
V-4Cr-4Ti	\$200 (plate form--average between 1994-1996 US fusion program large heats and Wah Chang 1993 “large volume” cost estimate)
Nb-1Zr	~\$100
Ta	\$300 (sheet form)
Mo	~\$80 (3 mm sheet); ~\$100 for TZM
W	~\$200 (2.3 mm sheet); higher cost for thin sheet

### 13.1.2 Overview of thermal stress capabilities of various alloys.

The key mechanical and physical properties of high-temperature refractory alloys and low-activation structural materials are summarized in Section 13.3. More detailed summaries of the properties for V-4Cr-4Ti, Fe-8-9Cr martensitic steel, SiC/SiC composites, and T-111 (Ta-8W-2Hf) are published elsewhere [fusion material semiannual refs.] and are posted on the APEX web site. A good summary of the properties for W is contained in the ITER Material Properties Handbook (pub. 4 and later versions) [1].

The allowable stress in refractory alloys is generally controlled by the ultimate strength rather than the yield strength (due to the low work hardening capacity of refractory alloys compared to, e.g., annealed austenitic stainless steel). In addition to the ultimate strength ( $\sigma_U$ ), the other key properties which determine the thermal stress resistance are the elastic modulus (E), Poisson's ratio ( $\nu$ ), thermal conductivity, ( $k_{th}$ ), and mean linear coefficient of thermal expansion ( $\alpha_{th}$ ). A thermal stress figure of merit convenient for qualitative ranking of candidate high heat flux structural materials is given by  $M = \sigma_U k_{th} (1 - \nu) / (\alpha_{th} E)$ . The maximum allowable heat flux is directly proportional to  $M/\sqrt{x}$ , where  $\sqrt{x}$  is the wall thickness. In addition, temperature limits (usually determined by thermal creep considerations) can be used for additional qualitative ranking of materials. A rigorous quantitative analyses of candidate materials requires the use of advanced structural design criteria such as those outlined in section 13.2.

The mechanical properties for recrystallized refractory alloys have been used as the reference case for purposes of APEX designs. The mechanical properties of stress-relieved (non-recrystallized) refractory alloys are superior to those of recrystallized specimens, with increases in strength of up to a factor of 2 being typical. However, the possibility of stress- or radiation-enhanced recrystallization of these alloys (along with the likely inclusion of welded joints in the structure) does not allow this strength advantage to be considered for conservative design analyses.

The thermal stress figures of merit varies from ~57 kW/m for a high strength, high conductivity CuNiBe alloy at 200°C [14] to ~2.0 for SiC/SiC at 800°C. Cu-Ni-Be is not suitable for structural use above ~300°C due to poor fracture toughness at elevated temperature [15], and the thermal creep strength of all copper alloys is low at temperatures above 400°C (0.5 $T_M$ ). Therefore, copper alloys are not attractive choices for high thermal efficiency power plants. The low thermal stress resistance of SiC/SiC is mainly due to the low thermal conductivity in currently available composites (primarily due to a combination of poor quality fibers and

imprecise control of the CVI deposition chemistry). The two major classes of low-activation structural alloys, V-Cr-Ti and Fe-8-9Cr martensitic steel have figures of merit of ~6.4 (450-700°C) and 5.4 (400°C), respectively. The refractory alloys offer some advantage over vanadium alloys and ferritic-martensitic steel, even in the recrystallized condition. For example, pure recrystallized tungsten has a figure of merit of  $M=11.3$  at 1000°C, and TZM (Mo-0.5Ti-0.1Zr) has a value of  $M=9.6$  at 1000°C. The alloy T-111 (Ta-8W-2Hf) has the best thermal stress figure of merit among the (non-copper) alloys considered, with a value of  $M=12.3$  at 1000°C. Nb-1Zr has an acceptable figure of merit ( $M=10.1$ ) at 600°C, but its strength and thermal stress capability decrease at temperatures above 600°C. Considering the high induced radioactivity of Nb compared to the other Group Vb alloys (V and Ta), the lack of a clear thermal stress performance advantage for Nb-1Zr makes this alloy less desirable for fusion energy structural applications compared to the other refractory alloys.

#### References

- [1] J.W. Davis, in: ITER Material Properties Handbook, ITER Document No. S74 MA 2 97-12-12 R 0.2, 4th ed, 1997.
- [2] F.W. Wiffen, in: Proc. Int. Conf. on Defects and Defect Clusters in BCC Metals and Their Alloys, Nuclear Metallurgy Vol. 18, ed. R.J. Arsenault, (National Bureau of Standards, Gaithersburg, MD, 1973) p. 176.
- [3] R.W. Buckman, Jr., in: High Temperature Silicides and Refractory Alloys, eds. C.L. Briant et al., MRS Symposium Proceedings vol. 322 (Materials Research Society, Pittsburgh, 1994) p. 329.
- [4] G.T. Murray, T.A. Lograsso, in: Metals Handbook, eds. J.R. Davis et al., vol. 2, Properties and Selection: Nonferrous Alloys and Special-Purpose Materials, 10th ed (ASM International, Materials Park, OH, 1990) p. 1091.
- [5] R.J. Farraro, R.B. McLellan, Metall. Trans. 10A (1979) 1699.
- [6] D.C. Goldberg, in: Aerospace Structural Metals Handbook, AFML-TR 68-115, ed. W.F. Brown, Jr., (Metals and Ceramics Information Center, Battelle Columbus Laboratories, 1969).
- [7] J.B. Conway, in: Proc. Symp. on Refractory Alloy Technology for Space Nuclear Power Applications, CONF-8308130, eds. R.H. Cooper, Jr., E.E. Hoffman, (Oak Ridge National Lab, 1984) p. 252.
- [8] T.E. Tietz, J.W. Wilson, Behavior and Properties of Refractory Metals, Stanford University Press, Stanford, CA, 1965.
- [9] J.B. Lambert, in: Metals Handbook, eds. J.R. Davis et al., vol. 2, Properties and Selection: Nonferrous Alloys and Special-Purpose Materials, 10 ed (ASM International, Materials Park, OH, 1990) p. 557.
- [10] M.A. Filyand, E.I. Semenova, Handbook of the Rare Elements, Vol. 2: Refractory Elements, Boston Tech. Publ., Boston, MA, 1970.
- [11] D.J. Senior, J.K. Thomas, K.L. Peddicord, J. Nucl. Mater. 173 (1990) 274.
- [12] D.J. Senior, J.K. Thomas, K.L. Peddicord, J. Nucl. Mater. 173 (1990) 261.
- [13] F.W. Wiffen, in: Proc. Symp. on Refractory Alloy Technology for Space Nuclear Power Applications, CONF-8308130, eds. R.H. Cooper, Jr., E.E. Hoffman (Oak Ridge National Lab, 1984) p. 252.
- [14] S.J. Zinkle, W.S. Eatherly, in: Fusion Materials Semiannual Progress Report for Period ending Dec. 31, 1996, DOE/ER-0313/21 (Oak Ridge National Lab, 1996) p. 165.

[15] D.J. Alexander, S.J. Zinkle, A.F. Rowcliffe, in: Fusion Materials Semiannual Progress Report for Period ending Dec. 31, 1996, DOE/ER-0313/21 (Oak Ridge National Lab, 1996) p. 175.

## 13.2 Structural Design Criteria

Most advanced blanket design concepts require the first wall to operate in temperature regimes where thermal creep effects may be important. Therefore, in addition to the usual low-temperature design rules, high-temperature design rules may also have to be applied. We have adopted the ITER Structural Design Criteria (ISDC) as a basis for the design rules to be used in APEX.

### 13.2.1 Definitions

Some of the key definitions needed during design calculations are included here; the rest can be obtained from the Section IRB of the ISDC.

**Primary stress:** primary stress is defined as that portion of the total stress which is required to satisfy equilibrium with the applied loading and which does not diminish after small scale permanent deformation.

**Secondary stress:** secondary stress is that portion of the total stress (minus peak stresses, as defined below), which can be relaxed as a result of small scale permanent deformation. The basic characteristic of a secondary stress is that it is self-limiting.

**Total stress (strain):** total stress  $\sigma_{ij}$  (strain  $\epsilon_{ij}$ ) is the stress (strain) under the effect of all the loadings to which the component is subjected.

**Membrane stress (strain):** membrane stress (or strain) tensor is the tensor whose components  $(\sigma_{ij})_m$   $[(\epsilon_{ij})_m]$  are equal to the mean value of stresses  $\sigma_{ij}$  ( $\epsilon_{ij}$ ) through the thickness.

**Bending stress (strain):** the bending stress (strain) tensor is that tensor whose components  $(\sigma_{ij})_b$   $[(\epsilon_{ij})_b]$  vary linearly through the thickness and which, when integrated through the thickness, have the same bending moment as the original tensor  $\sigma_{ij}(\epsilon_{ij})$ .

**Peak stress:** Peak stress is the increment of stress which is additive to the membrane-plus-bending stresses by reason of local discontinuities or local thermal stresses including the effects, if any, of stress concentrations.

**Stress intensity:** the stress intensity,  $\bar{\sigma}$ , at any given point is a scalar derived from the stress tensor,  $\sigma$ , at that point, using the following maximum shear or Tresca criterion:

$$\bar{\sigma} = \max (|\sigma_1 - \sigma_2|, |\sigma_2 - \sigma_3|, |\sigma_3 - \sigma_1|)$$

where  $\sigma_1$ ,  $\sigma_2$ , and  $\sigma_3$  are the principal stresses.

**Effective stress:** the effective stress used for creep calculation is based on von-Mises effective stress, i.e.,

$$\sigma_e = \sqrt{1/2} \cdot \left\{ (\sigma_{11} - \sigma_{22})^2 + (\sigma_{22} - \sigma_{33})^2 + (\sigma_{33} - \sigma_{11})^2 + 6 (\sigma_{12}^2 + \sigma_{23}^2 + \sigma_{31}^2) \right\}^{1/2}$$

**Stress intensity range:** it is the maximum of the stress intensities of the tensor differences between the stress tensors  $\sigma(t)$  and  $\sigma(t')$  for every pair of times  $t$  and  $t'$  within a cycle.

**Allowable primary membrane stress intensity ( $S_m$ ):**  $S_m$  is a temperature (T) and fluence ( $\Phi t$ )

dependent allowable stress intensity defined as the least of the following quantities:

$$\text{Min}[1/3S_{u,\min}(\text{RT}, 0), 1/3S_{u,\min}(T, 0), 1/3S_{u,\min}(T, \Phi t), 2/3S_{y,\min}(\text{RT}, 0), 2/3S_{y,\min}(T, 0), 2/3S_{y,\min}(T, \Phi t)],$$

where  $S_{y,\min}$  and  $S_{u,\min}$  are the minimum yield and ultimate tensile strengths, respectively, and RT is room temperature.

**Uniform elongation ( $e_u$ ):**  $\epsilon_u$  is defined as the plastic component of the engineering strain at the time when necking begins in a uniaxial tensile test.

**True strain at rupture ( $e_{tr}$ ):**  $\epsilon_{tr}$  is defined as :

$$\epsilon_{tr} = \ln \left( \frac{100}{100 - \%RA} \right),$$

where %RA is the reduction in area (%) as determined in a uniaxial tension test at a given temperature, strain rate, and fluence.

**Elastic follow-up factor (r):** the r-factor provides a simplified inelastic analysis approach by which the peak inelastic strain and stress in a structure can be estimated from elastic analysis results. An r value =4 is used in ISDC as a conservative estimate for many structures made of ductile alloys with adequate strain-hardening capability. For irradiated materials with severe loss of strain hardening capability (uniform elongation), r can be much larger.

**Allowable primary plus secondary membrane stress intensity ( $S_e$ ):**  $S_e$  is a temperature (T) and fluence ( $\phi t$ ) dependent allowable stress intensity for a material with severe loss of uniform elongation due to irradiation and is defined as follows:

$$S_e = \frac{1}{3} \left[ S_{u,\min}(T, \phi t) + \frac{E \alpha_1}{r_1} (\epsilon_u(T, \phi t) - 0.02) \right] \quad \text{if } \epsilon_u(T, \phi t) = 2\%$$

and

$$S_e = \frac{1}{3} S_{u,\min}(T, \phi t) \quad \text{if } \epsilon_u(T, \phi t) < 2\%$$

where E is Young's modulus,  $\alpha_1 = 0.5$ , and

$$r_1 = \begin{cases} \infty & \text{for } \epsilon_u \leq .02 \text{ (2\%)} \\ 4 & \text{for } \epsilon_u > .02 \end{cases}$$

**Allowable total stress intensity ( $S_d$ ):**  $S_d$  is a temperature (T), fluence ( $\phi t$ ), and r-factor dependent allowable stress intensity for total primary plus secondary stress in radiation embrittled materials, and is defined as follows:

$$S_d = \frac{2}{3} \left( S_{u,\min}(T, \phi t) + \frac{E}{r} \frac{\epsilon_{tr}(T, \phi t)}{TF} \right)$$

where

TF = triaxiality factor to account for the effect of hydrostatic stress on ductility,

$$= \frac{\sqrt{2} (\sigma_1 + \sigma_2 + \sigma_3)}{\left[ (\sigma_1 - \sigma_2)^2 + (\sigma_2 - \sigma_3)^2 + (\sigma_3 - \sigma_1)^2 \right]^{1/2}},$$

$r$  = elastic follow-up factor whose value is  $r_2$  in zones of stress concentration (i.e., peak stress due to stress concentration is included), and  $r_3$  away from zones of stress concentration.

$$r_2 = \text{Max} \{K_T \text{ and } 4\}$$

where  $K_T$  is the elastic stress concentration factor and

$$r_3 = \begin{cases} \infty & \text{for } \epsilon_u \leq .02 \text{ (2\%)} \\ 4 & \text{for } \epsilon_u > .02 \end{cases}$$

**Time-dependent allowable primary stress intensity ( $S_t$ ):**  $S_t$  is a time and temperature-dependent allowable primary stress intensity defined as the least of the following:

- (1) two thirds of the minimum stress corresponding to average creep rupture time  $t$  at temperature  $T$ ,
- (2) 80% of the minimum stress corresponding to time  $t$  and temperature  $T$  for onset of tertiary creep, and
- (3) minimum stress to cause a creep strain of  $\min[1\%, \epsilon_C/5]$  in time  $t$  and temperature  $T$ , where  $\epsilon_C$  is the minimum creep ductility.

### Design rules

Since the design studies under APEX are preliminary in nature, only elastic analysis design rules are included. For full inelastic analysis design rules, the IRB Section of the ISDC may be used. The design rules are divided into a high temperature section and a low temperature section, depending on whether thermal creep effects are or are not important. The low temperature rules are always applicable. To determine whether the high temperature rules are also to be applied, the following negligible creep test should be used.

### Negligible creep test

Thermal creep is negligible over the total design lifetime of a component if the following summation limit is satisfied:

$$\sum_{i=1}^N \left( \frac{t_i}{t_{c_i}} \right) \leq 1 \quad (1)$$

where the total lifetime is divided into  $N$  intervals of time; for each interval  $i$ , of duration  $t_i$ , the maximum temperature is denoted by  $T_i$ . The negligible thermal creep time  $t_{c_i}$  at a temperature  $T_i$  is calculated as the time required to accumulate a thermal creep strain of 0.05% in a uniaxial creep specimen subjected to a constant stress of  $1.5 S_m(T_i)$ . If inequality (1) is satisfied, then only low temperature design rules need be applied.

### Low temperature design rules

#### Necking and plastic instability limits

To prevent failure by necking and plastic instability, the following limits must be satisfied at all times:

$$\frac{P_m}{P_L + P_b} \leq S_m(T_m, \phi t_m) \quad (2a)$$

$$P_L + P_b \leq K S_m(T_m, \phi t_m) \quad (2b)$$

where  $P_m$  is general primary membrane stress,  $P_L$  is local primary membrane stress,  $P_b$  is primary bending stress,  $K$  is bending shape factor ( $= 1.5$  for solid rectangular section), and  $S_m$  is evaluated at the thickness-averaged temperature ( $T_m$ ) and fluence ( $\phi t_m$ ).

### Plastic flow localization limit

To prevent cracking due to plastic flow localization (in a material with significant loss of uniform elongation due to irradiation), the following limit must be satisfied at all times during the life of the component:

$$\overline{P_L + Q_L} \leq S_e(T_m, \phi t_m) \quad (3)$$

where  $Q_L$  is the secondary membrane stress.

### Ductility exhaustion limits

To prevent local fracture due to exhaustion of ductility (due to embrittlement), the following limits must be satisfied at all times during the life of the component:

The total stress, including peak stress, is limited by

$$\overline{P_L + P_b + Q + F} \leq S_d(T, \phi t, r_2) \quad (4a)$$

where  $F$  is peak stress (e.g., due to stress concentration), and the total stress, excluding peak stress, is limited by

$$\overline{P_L + P_b + Q} \leq S_d(T, \phi t, r_3). \quad (4b)$$

### Brittle fracture limit

To prevent brittle fracture initiating from severe flaws or notches, the maximum mode I stress intensity factor,  $K_I$ , due to all primary and secondary loadings, including peak ( $P_L + P_b + Q + F$ ), must be limited by the following:

$$K_I \leq K_C(T_m, \Phi t_m) \quad (5)$$

where  $K_C$  is the linear-elastic fracture toughness evaluated at the thickness-averaged temperature and fluence. The stress intensity factor  $K_I$  has to be determined from the analysis of a postulated surface flaw of depth  $a_0$ , length  $4a_0$ , where  $a_0 = \max[4a_u, h/4]$ ,  $a_u$  = largest undetectable crack length, and  $h$  = section thickness. If the full section under consideration (without the flaw) experiences plasticity, a suitable non-linear fracture parameter (e.g., J-integral) should be used instead of  $K$ .

### Ratcheting limits

To prevent ratcheting due to cyclic loading, either of the following two limits should be satisfied at all times:

$3S_m$  limit

$$(\overline{P_L + P_b})_{\max} + \Delta[\overline{P} + \overline{Q}]_{\max} \leq 3S_m(T_m, \phi t_m) \quad (6)$$

where  $\Delta$  denotes range of primary ( $P$ ) or secondary ( $Q$ ) stress due to cyclic loading.

Bree-diagram limit

$$Y \leq \begin{cases} \frac{1}{X} & \text{for } 0 \leq X \leq 0.5 \\ 4(1 - X) & \text{for } 0.5 < X \leq 1 \end{cases} \quad (7a)$$

where

$$X = \frac{\overline{P_m}}{S_y} \quad \text{or} \quad X = \frac{\overline{P_L + \frac{P_b}{K}}}{S_y} \quad \text{and} \quad Y = \frac{\Delta[\overline{P} + \overline{Q}]}{S_y}, \quad (7b)$$

and the yield stress  $S_y$  is evaluated at the average of the thickness-averaged temperatures at the “cold” and “hot” ends of the cycle.

### Fatigue limit

To prevent the initiation of a fatigue crack due to cyclic loading, the fatigue usage fraction  $V$  at the end of life must satisfy the following limit

$$V = \sum_{j=1}^J \frac{n_j}{N_j(\overline{\Delta\epsilon_j})} < 1 \quad (8)$$

where the lifetime is divided into  $J$  type of cycles. For each cycle type  $j$ , characterized by  $n_j$  cycles at an equivalent strain range  $\overline{\Delta\epsilon_j}$  and average temperature  $T_j$  during the cycle,  $N_j$  is the allowable cycles. If  $\overline{\Delta\epsilon_j}$  is calculated elastically, it should be corrected for possible plasticity effects (e.g., by Neuber's rule for notches).

### High temperature design rules

#### Creep damage limits

To guard against creep damage, the following limits must be satisfied:

$$\overline{P_m} \leq S_t(T_m, t) \quad (9a)$$

$$\overline{P_L + P_b / K_t} \leq S_t(T_m, t) \quad (9b)$$

where  $t$  is the design lifetime, and  $K_t = (K+1)/2$ . If the lifetime involves variable stress and temperature history, Eqs.9a-b should be replaced by limits on usage fraction sums.

#### Creep-ratcheting limit

If the negligible creep test (Eq. 1) is not satisfied, then in addition to satisfying the low temperature ratcheting limit based on Bree diagram (Eq. 7a), the high temperature ratcheting limit should be satisfied by first calculating an effective core stress  $\sigma_c$  for creep calculations as follows:

$$\sigma_c = Z S_{yL} \quad (10)$$

where  $S_{yL}$  is the  $S_y$  value at the "low" temperature extreme of the cycle and  $Z$  is a creep stress parameter defined in terms of  $X$  and  $Y$  (which are defined in Eq. 7b),

$$Z = X \text{ for } X + Y = 1 \quad (11a)$$

$$Z = Y + 1 - 2\sqrt{(1 - X)Y} \text{ for } 1 - X = Y < 1/(1 - X) \quad (11b)$$

$$Z = XY \text{ for } Y > 1/(1 - X) \quad (11c)$$



The total creep strain accumulated during the lifetime due to a stress  $1.25\sigma_c$  should be less than  $\min[1\%, \epsilon_c/5]$  where  $\epsilon_c$  is the minimum creep ductility during the cycle. If the lifetime involves more than one types of cycles of stress and temperature, the criterion is satisfied by the use of usage fraction sums.

### **Creep-fatigue limit**

If the negligible creep test (Eq. 1) is not satisfied, then creep damage (W) has to be added to the fatigue damage (V) as evaluated in Eq. 8, i.e.,

$$V+W < 1 \quad (12)$$

where W is the creep damage obtained by first dividing the lifetime into K intervals. Each interval k of duration  $\Delta t_k$  is characterized by a maximum temperature  $T_k$ , a maximum effective stress  $\sigma_{e,k}$ . The following sum defines the creep damage W:

$$W = \sum_k \frac{\Delta t_k}{t_{R,k}} \quad (13)$$

where  $t_{R,k}$  is the minimum time to creep rupture at temperature  $T_k$  and stress  $1.25\sigma_{c,k}$ .

## **13.3 Summary of thermophysical properties (unirradiated and irradiated)**

The following tables provide analytical expressions for the temperature-dependent mechanical and thermophysical properties for five of the structural materials considered for APEX. The analytical expressions were determined from least-squares fits of experimental data. Further details are available at the APEX web site and in references 1-4.

### **Section 13.3 References:**

- [1] S.J. Zinkle, in: Fusion Materials Semiann. Prog. Report for period ending Dec. 31 1997, DOE/ER-0313/23 (Oak Ridge National Lab, 1997) p. 99.
- [2] S.J. Zinkle, J.P. Robertson, R.L. Klueh, in: Fusion Materials Semiann. Prog. Report for period ending June 30 1998, DOE/ER-0313/24 (Oak Ridge National Lab, 1998) p. 135.
- [3] S.J. Zinkle, L.L. Snead, in: Fusion Materials Semiann. Prog. Report for period ending June 30 1998, DOE/ER-0313/24 (Oak Ridge National Lab, 1998) p. 93.
- [4] J.W. Davis, in: ITER Material Properties Handbook, ITER Document No. S74 MA 2 97-12-12 R 0.2, 4 ed, 1997.

### **Summary of V-4Cr-4Ti Properties**

#### **Ultimate Tensile Strength (unirradiated)**

$$\sigma_{UTS}(\text{MPa}) = 446 - 0.806*T + 0.00221*T^2 - 1.79e-06*T^3 + 1.82e-10*T^4 \quad (T \text{ in } ^\circ\text{C})$$

#### **Yield Strength (Unirradiated)**

$$\sigma_Y(\text{MPa}) = 377 - 0.704*T + 0.00090*T^2 - 1.23e-07*T^3 - 1.98e-10*T^4 \quad (T \text{ in } ^\circ\text{C})$$

### **Elongation**

$e_{\text{tot}}$ , RA are high in unirradiated and irradiated conditions

$e_u$  is high in unirradiated conditions, moderate (>2%) after irradiation at  $T > 430^\circ\text{C}$  and low (<1%) for irradiation at  $T < 400^\circ\text{C}$

### **Elastic constants**

$$E_Y \text{ (GPa)} = 128 - 0.00961 * T \quad (T \text{ in Kelvin})$$

$$G \text{ (GPa)} = 48.8 - 0.00843 * T \quad (T \text{ in Kelvin}) \quad \nu = (E_Y / 2G) - 1$$

### **Thermophysical properties**

$$\alpha_{\text{th}} = 9.03767 + 0.00301422 * T + 4.95937 \times 10^{-7} * T^2 \quad \text{ppm}/^\circ\text{C} \quad (T \text{ in } ^\circ\text{C})$$

$$C_P = 0.5755 - 21.1 / T \quad \text{J/g-K} \quad (T \text{ in Kelvin})$$

$$k_{\text{th}} = 27.8 + 0.0086 T \quad \text{W/m-K} \quad (T \text{ in Kelvin})$$

### **Recommended operating temperature limits (structural applications)**

$T_{\text{min}} = 400^\circ\text{C}$  (due to rad.-induced increase in DBTT at low  $T_{\text{irr}}$ )

$T_{\text{max}} = 700^\circ\text{C}$  (corrosion/chemical compatibility and thermal creep)

### **Summary of 8-9Cr Ferritic/Martensitic Steel Properties**

#### **Ultimate Tensile Strength (unirradiated)**

$$\sigma_{\text{UTS}} \text{ (MPa)} = 683 - 1.162 * T + 0.00547 * T^2 - 1.17 \times 10^{-5} * T^3 + 6.24 \times 10^{-9} * T^4 \quad (T \text{ in } ^\circ\text{C})$$

#### **Yield Strength (Unirradiated)**

$$\sigma_Y \text{ (MPa)} = 531 - 0.388 * T + 0.00148 * T^2 - 2.40 \times 10^{-6} * T^3 - 1.45 \times 10^{-10} * T^4 \quad (T \text{ in } ^\circ\text{C})$$

### **Elongation**

$e_{\text{tot}}$ , RA are moderate to high in unirradiated and irradiated conditions ( $e_{\text{tot}} \sim 8\text{-}10\%$  for  $T_{\text{irr}} < 400^\circ\text{C}$ )

$e_u$  is low in unirradiated (0.2-7%) and irradiated (<3%) conditions

### **Elastic constants**

$$E_Y \text{ (GPa)} = 233 - 0.0558 * T \quad 20\text{-}450^\circ\text{C} \quad (T \text{ in Kelvin})$$

$$G \text{ (GPa)} = 90.1 - 0.0209 * T \quad 20\text{-}450^\circ\text{C} \quad (T \text{ in Kelvin}) \quad \nu = (E_Y / 2G) - 1$$

### **Thermophysical properties**

$$\alpha_{\text{th}} = 10.4 \text{ ppm}/^\circ\text{C} (20^\circ\text{C}) \text{ to } 12.4 \text{ ppm}/^\circ\text{C} (700^\circ\text{C})$$

$$C_P = 0.47 \text{ J/g-K} (20^\circ\text{C}) \text{ to } 0.81 \text{ J/g-K} (700^\circ\text{C})$$

$$k_{\text{th}} = 33 \text{ W/m-K} \quad (20\text{-}700^\circ\text{C})$$

### **Recommended operating temperature limits (structural applications)**

$T_{\text{min}} = 250^\circ\text{C}$  (due to rad.-induced increase in DBTT at low  $T_{\text{irr}}$ )

$T_{\text{max}} = 550^\circ\text{C}$  (thermal creep);  $T_{\text{max}} \sim 700^\circ\text{C}$  for ODS steels?

### **Summary of SiC/SiC Properties**

#### **Ultimate Tensile Strength (unirradiated)**

$\sigma_{UTS} \sim 220\text{-}240 \text{ MPa}$  (20-1000°C)

#### **Proportional Limit Strength (Unirradiated)**

$\sigma_Y(\text{MPa}) \sim 70 \text{ MPa}$  (20-1000°C)

#### **Elongation**

$e_{tot}$ ,  $e_u$ , RA are very low in unirradiated and irradiated conditions

#### **Elastic constants**

$E_Y \text{ (GPa)} \sim 400 \text{ GPa}$  20- 1000°C (Sylramic or Hi-Nicalon type S fibers, 10% matrix porosity)

$G \text{ (GPa)} \sim 165 \text{ GPa}$  20- 1000°C

$\nu = 0.16$  20- 1000°C

#### **Thermophysical properties**

$\alpha_{th} \sim 2.5 \text{ ppm/}^\circ\text{C}$  (20°C) to  $4.5 \text{ ppm/}^\circ\text{C}$  (1000°C)

$C_P = 1110 + 0.15 T - 425 e^{-0.003T} \text{ J/kg-K}$  (1000°C)

$k_{th} = 10\text{-}15 \text{ W/m-K}$  (400-1000°C, after irradiation)

#### **Recommended operating temperature limits (structural applications)**

$T_{min} \sim 500^\circ\text{C}$ ? (due to rad.-induced decrease in thermal conductivity)

$T_{max} = 1000^\circ\text{C}$ ? (due to cavity swelling)

### **Summary of Recrystallized Ta-8W-2Hf (T-111) Properties**

#### **Ultimate Tensile Strength (unirradiated)**

$\sigma_{UTS}(\text{MPa}) = 630 - 1.532 * T + 0.003388 * T^2 - 2.807e-06 * T^3 + 7.338e-10 * T^4$  (T in °C)

#### **Yield Strength (Unirradiated)**

$\sigma_Y(\text{MPa}) = 612 - 1.743 * T + 0.003585 * T^2 - 3.076e-06 * T^3 + 8.819e-10 * T^4$  (T in °C)

#### **Elongation**

$e_{tot}$ , RA are high in unirradiated and irradiated conditions

$e_u$  is high in unirradiated conditions, moderate (>2%) after irradiation at  $T > 650^\circ\text{C}$

and low (<1%) for irradiation at  $T < 600^\circ\text{C}$

#### **Elastic constants (pure Ta)**

$E_Y \text{ (GPa)} = 169 - 0.00822 * T - 1.66 \times 10^{-6} T^2$  (T in Kelvin)

$G \text{ (GPa)} = 77.4 - 0.0173 * T$  (T in Kelvin)  $\nu = (E_Y/2G) - 1$

$\nu = 0.35$  (300 K)

#### **Thermophysical properties**

$\alpha_{th} = 5.9 \text{ ppm/}^\circ\text{C}$  (20°C) and  $7.6 \text{ ppm/}^\circ\text{C}$  (1650°C)

$C_P = 150 \text{ J/kg-K}$  (20°C)

$$K_{th} \text{ (W/m-K)} = 41.0 + 0.020 T - 6.32 \times 10^{-6} T^2 \quad (T \text{ in } ^\circ\text{C})$$

### **Recommended operating temperature limits (structural applications)**

$T_{min} = 650^\circ\text{C}$  (due to radiation-induced increase in DBTT at low  $T_{irr}$ )

$T_{max} = 1200^\circ\text{C}$  (thermal creep)

### **Summary of Recrystallized W-(5-10%) Re Properties**

#### **Ultimate Tensile Strength (unirradiated)**

$\sigma_{UTS} \text{ (MPa)} = 377.9 + 0.03207 * T - 1.955 \times 10^{-4} * T^2 + 5.13 \times 10^{-8} * T^3$  (T in  $^\circ\text{C}$ ) –used pure W values

#### **Yield Strength (Unirradiated)**

$\sigma_Y \text{ (MPa)} = 94.2 - 0.0214 * T - 2.12 \times 10^{-6} * T^2 - 7.48 \times 10^{-10} * T^3$  (T in  $^\circ\text{C}$ ) –used pure W values

#### **Elongation**

$e_{tot} \text{ (%) } = 20.8 + 0.053 * T - 2.18 \times 10^{-5} * T^2$  (T > 500 $^\circ\text{C}$ ) --used pure W values

#### **Elastic constants**

$E_Y \text{ (GPa)} = 398 - 0.00231 * T - 2.72 \times 10^{-5} T^2$  (T in  $^\circ\text{C}$ ) --pure W values; W-25Re

$E(20^\circ\text{C}) = 410 \text{ GPa}$

$\nu = 0.279 + 1.09 \times 10^{-5} T$  (T in  $^\circ\text{C}$ ) W-25Re  $\nu(20^\circ\text{C}) = 0.30$ ,

$G(20^\circ\text{C}) = 159 \text{ GPa}$

#### **Thermophysical properties**

$\alpha_m \text{ (} 10^{-6}/^\circ\text{C)} = 3.9 + 5.8 \times 10^{-5} * T + 5.7 \times 10^{-11} * T^2 - 2.0 \times 10^{-14} * T^3$  (T in  $^\circ\text{C}$ ) --used pure W values

$C_P \text{ (J/kg-K)} = 128 + 0.033 * T - 3.4 \times 10^{-6} * T^2$  ??? (T in  $^\circ\text{C}$ ) --used pure W values

$K_{th} \text{ (W/m-K)} \sim 85 \text{ W/m-K}$  (1000-2400 $^\circ\text{C}$ ) --conductivity decreases with increasing Re content

### **Recommended operating temperature limits (structural applications)**

$T_{min} = 800^\circ\text{C}$  (due to radiation-induced increase in DBTT at low  $T_{irr}$ )

$T_{max} = 1400^\circ\text{C}$  (Li, Pb-Li corrosion/chemical compatibility and thermal creep)

#### **13.3.1. Overview of Radiation Effects in Refractory Metals**

- Void swelling is not anticipated to be a lifetime-limiting issue due to the BCC structure of the high-temperature refractory alloys
  - existing fission reactor data base indicate moderate swelling (<2%) for doses up to 10 dpa or higher
  - effects of fusion-relevant He generation on swelling is uncertain
  - swelling regimes are ~600 to 1000 $^\circ\text{C}$  for all 4 classes of refractory alloys

- Radiation hardening can lead to a large increase in the ductile to brittle transition temperature. The radiation hardening in BCC alloys at low temperatures ( $<0.3T_M$ ) is typically pronounced even for doses of  $\sim 1$  dpa. The amount of radiation hardening typically decreases rapidly with irradiation temperature above  $0.3T_M$ , and radiation-induced increases in the DBTT may be anticipated to be acceptable at temperatures above  $\sim 0.3 T_M$  (although experimental verification is needed).
- The Group Vb alloys (V, Nb, Ta) exhibit better ductility before and after irradiation compared to Mo, W
  - very limited mechanical properties data base on irradiated Nb, Ta alloys (qualitative trends can be inferred from the larger database on irradiated V alloys)
  - a moderate mechanical properties data base exists for irradiated Mo alloys (but at relatively low irradiation temperatures); the irradiated W database is very limited
- Very limited or no fracture toughness/Charpy impact data exist on irradiated high temperature refractory alloys
  - “tensile DBTT” of Mo, W alloys increases to very high values even for low dose irradiations at moderate temperatures (e.g.,  $600^\circ\text{C}$  after  $\sim 1$  dpa irradiation at  $300^\circ\text{C}$  for W, W-10Re)
- radiation-enhanced recrystallization and/or radiation creep effects need to be investigated

#### Ta Alloys: T-111 (Ta-8W-2Hf)

- Significant radiation hardening at  $415, 640^\circ\text{C}$  ( $\sigma_y$ , UTS  $>1000$  MPa) after  $1.9 \times 10^{26}$  n/m<sup>2</sup>,  $E > 0.1$  MeV (2.5 dpa Ta, 10 dpa steel) -- Wiffen 1984
- Very little radiation hardening at  $800^\circ\text{C}$  (Wiffen 1984)

=> estimated minimum operating temperature  $\sim 650^\circ\text{C}$ , based on DBTT considerations

#### Mo Alloys: TZM, etc. (largest irradiated data base among high temperature refractories)

- Pronounced radiation hardening up to  $\sim 600^\circ\text{C}$ , 7-34 dpa; tensile strength after irradiation at  $800^\circ\text{C}$ , 11 dpa was  $\sim 1000$  MPa (Hasegawa et al. 1995, 1996)
- Tensile elongation  $\sim 0$  for  $T_{irr} < 700^\circ\text{C}$ , 5-20 dpa in Mo, TZM, Mo-Re alloys (Steichen 1976, Chakin&Kazakov 1996, Fabritsiev & Pokrovsky 1998)
- Tensile “embrittlement” observed in Mo-Zr-B for  $T_{irr} = 750-850^\circ\text{C}$ ,  $\sim 10$  dpa; “tensile DBTT” decreased rapidly for  $T_{irr} > 900^\circ\text{C}$  (Chakin&Kazakov 1996)
- Irradiation data at doses  $> 0.1$  dpa are not yet available for “radiation embrittlement-resistant” Mo-TiC alloys; impact bending specimens are not notched (Kurishita et al. 1996)
- No known fracture toughness data on irradiated specimens

=> estimated minimum operating temperature ~750°C, based on DBTT considerations

#### W and W Alloys: P/M or CVD W, W-1% La<sub>2</sub>O<sub>3</sub>, W-Mo-Y (alloy W-13I)

- Tensile elongation ~0 for T<sub>irr</sub>= 400, 500°C, 0.5-1.5x10<sup>26</sup> n/m<sup>2</sup>, ≤2 dpa (Steichen 1976, Wiffen 1984, Gorynin et al 1992); irradiations at 700°C are in progress
- Un-notched bend bar DBTT>900°C for W, W-10%Re irradiated at 300°C, 0.5x10<sup>26</sup> n/m<sup>2</sup>, (~1 dpa); most rapid embrittlement observed for W-10%Re (Krautwasser et al 1990)

=> estimated minimum operating temperature ≥800°C, based on DBTT considerations (scaling from Mo alloy data base)

### 13.4 Coolant/structure chemical compatibility

#### Chemical Compatibility of High Temperature Refractory Alloys with Liquid Metals and Flibe

- In general, the refractory alloys have very good compatibility with the liquid metals and salts of interest for fusion applications
  - impurity pickup is the key engineering issue
- Li chemical compatibility data base:
  - T-111 (Ta-8W-2Hf) data up to 1370°C (good compatibility; static and circulating loops)
  - Nb-1Zr data up to 1000°C (good compatibility; static and circulating loops)
  - W alloys up to 1370°C (attack observed at ≥1540°C)
  - Mo alloys (TZM) up to 1370°C (attack observed at ≥1540°C)
- Chemical compatibility data base for Flibe  
(generally good compatibility with proposed structural metals)

The focus of this section is on the chemical compatibility issues between structural materials and coolants, with particular emphasis on volatile oxidation of Group V and VI refractory alloys.

#### 13.4.1 Temperature and Oxygen Partial Pressure Limits for Mo and W Alloys

At low temperatures and pressures, the chemical reactions of a gas with a solid generally result in the formation of solid corrosion products. However, at elevated temperatures and low oxygen partial pressures, the formation of volatile corrosion products is thermodynamically favored. The chemical compatibility issues are examined based on thermodynamic and non-equilibrium analysis to estimate upper bounds for operating temperatures and oxygen partial pressures in the He-coolant.

The approach to model the high-temperature oxidation is to use a quasi-equilibrium treatment of heterogeneous reactions for the systems oxygen-W and oxygen-Mo. The rate-limiting step in

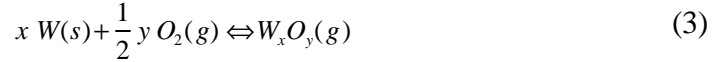
these reactions is the trapping (adsorption) of oxygen atoms until equilibrium is reached. Assuming that the helium pressure is  $P_{sys}$  and the gas temperature is  $T^*$ , the oxygen partial pressure ( $P_{O_2}$ ) is given by:

$$P_{O_2} = appm \times 10^{-6} P_{sys} \quad (1)$$

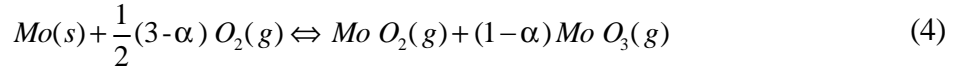
The adsorption of oxygen depends on the oxygen impingement ( $Z_{O_2}$ ) per unit area of wall surface, given by:

$$Z_{O_2} = P_{O_2} \sqrt{2\pi M_{O_2} RT} \quad (2)$$

where  $M_{O_2}$  is the molar weight of oxygen,  $R$  is the universal gas constant and  $T$  is in K. For W, the thermodynamic reactions take place based on:



A similar reaction describes the oxidation of Mo, however, at temperatures between 1500 and 2500K the reaction is more precisely described by:



The formation enthalpies and entropies of the oxides of Mo and W are given in Table 1. The quasi-equilibrium treatment of oxidation is based on the method developed by Batty and Stickney [1]. The principal parameter in the quasi-equilibrium treatment is the equilibration probability,  $\zeta$ , which depends on the probability of the impinging molecule  $s$  to have sufficient energy to surmount the activation barrier. If  $\zeta_{O_2}$  represents the probability that an impinging molecule will be equilibrated, then the rate of adsorption or equilibration  $\Gamma_{O_2}$  is:

$$\Gamma_{O_2} = \zeta_{O_2} Z_{O_2} \quad (5)$$

where  $Z_{O_2}$  is the impingement rate of  $O_2$  molecules on the surface given by equation (2). Letting  $i$  be  $W_x O_y$  and the Gibbs Free energy be:

$$\Delta G_i(T) = \Delta H_i(T) - T \Delta S_i(T) \quad (6)$$

the following system of equations can be solved for the partial pressure of oxygen, which results in the equilibration of the impinging oxygen molecules on the wall:

$$\begin{aligned} K_i &= \frac{P_i}{(P_{O_2})^{y/2}} = \exp(-\Delta G_i(T) / RT) \quad i = 1, 2, \dots, N \\ P_{O_2} &= \sqrt{P_{O_2}} \exp(-\Delta G_{O_2} / RT) \\ P_{O_2} &= P_{O_2} + P_{O_2} + \sum_1^N P_i \end{aligned} \quad (7)$$

The equilibration probabilities have been established for W:

$$\zeta_{O_2} = \exp[10.3498 - \frac{2.7607 \times 10^4}{T}] \quad (8)$$

and for Mo:

$$Z_{O_2} = 3.2 \times 10^4 \times 10^{-1.186 \times 10^4 / T} \quad (9)$$

where  $T$  is in K.

Mass-spectrometric investigations of gas-solid chemical reactions resulting in the formation of volatile W-oxides and Mo-oxides can be found in references [2-5] and [6-8], for W and Mo, respectively. An example of evaporation rate measurements for W-oxides [2] is shown in Fig. 1. All measurements show a distinct maximum for W at around 2200 K. The set of equations

given above have been solved to determine the erosion rate by volatile oxidation for the W and Mo system. Estimates for the evaporation rate of W and Mo under typical APEX operating conditions (10 MPa helium; 1ppm oxygen) are shown in Fig. 2. Similar to the measurements the W evaporation rate also reaches a maximum value at 2200 K and that of Mo reaches an asymptotic maximum around the same temperature. However, the estimated rates of evaporations are well above any experimental findings. The reason for the higher predicted evaporation rates is that the boundary layer effects on inhibition of the evaporated oxides in a moving coolant are not reflected in the above model.

Table 1: Enthalpies and Entropies for W and Mo.

<b>Tungsten</b>		<b>Molybdenum</b>		
<b>Species</b>	<b>DHf<sub>298.15</sub> (kcal/g.mole)</b>	<b>Species</b>	<b>DHf<sub>298.15</sub> (kcal/g.mole)</b>	<b>DSf<sub>298.15</sub> (cal/g.mole.K)</b>
O(g)	59.559	O(g)	61.3	16
W O(g)	101.6	Mo O(g)	95	25.5
WO <sub>2</sub> (g)	18.3	MoO <sub>2</sub> (g)	11.0	9.0
W O <sub>3</sub> (g)	-70.0	Mo O <sub>3</sub> (g)	-80	-15.5
W <sub>2</sub> O <sub>6</sub> (g)	-278.2	Mo <sub>2</sub> O <sub>6</sub> (g)	-270	-72
W <sub>3</sub> O <sub>8</sub> (g)	-408.7	Mo <sub>3</sub> O <sub>8</sub> (g)	-400	-118
W <sub>3</sub> O <sub>9</sub> (g)	-483.6	Mo <sub>3</sub> O <sub>9</sub> (g)	-463	-132
W <sub>4</sub> O <sub>12</sub> (g)	-670.2	Mo <sub>4</sub> O <sub>12</sub> (g)	-640	-190



## BOUNDARY LAYER EFFECTS

Under laminar flow conditions, the oxygen impingement rate can be significantly lower compared with a static coolant. The reason is the formation of a boundary layer, which adds resistance for the impinging oxygen. To estimate the effects of the boundary layer the collisional and the boundary layer resistances have to be estimated. The kinetic or collisional impingement rate has to balance the boundary layer diffusion rate. This condition allows the formulation of a “blowing” factor or the reduction in oxygen impingement rate because of the existence of the laminar boundary. The following set of equations provide the boundary layer resistance ( $R_B$ ) term:

$$\begin{aligned} R_B &\cong \frac{P_t}{r_g V St_m f_b} \\ St_m &= 0.0296 Re^{-0.2} Sc_i^{-0.4} \\ Sc_i &= 0.145 M_i^{0.556} \end{aligned} \quad (11)$$

where  $St_m$  is the Stanton number and  $Sc_i$  is the Schmidt number.

The kinetic resistance ( $R_k$ ) term is given by:

$$R_{Ki} = \sqrt{\frac{2\pi RT_s}{M_i}} \quad (11)$$

Using the boundary layer and the collisional resistances the surface recession (X) rate is determined as:

$$\left( \frac{dX}{dt} \right)_{Boundary} = \frac{\left( \frac{dX}{dt} \right)_{Kinetic}}{1 + \frac{R_B}{R_k}} \quad (12)$$

The results of applying the effects of the boundary resistance to the recession rate of W and Mo are shown in Figures 3 and 4.

The effect of a boundary layer resistance to the oxygen impingement rate and the inhibition of the evaporated oxides of W and Mo can result in several orders of magnitude reduction of evaporation rates. The above model does not take into account many of the physical features of real wall-coolant interactions, such as, roughness, bends, and temperature variations along the flow. These issues will affect the final evaporation rate, however it is reasonable to assume that the evaporation rate of W and Mo will be below a few microns per year, when operated in a temperature range between 1200 and 1300°C.

## SUMMARY

Formation of volatile oxides can lead to pronounced surface erosion of Group VI metals (Mo, W) at elevated temperatures. The evaporation rate increases rapidly up to ~2000K in both Mo and W. If boundary layer scattering effects are ignored, the evaporation rate exceeds 100  $\mu\text{m/y}$

at ~1500 K in both materials for 1 ppm oxygen in He at a pressure of 10 MPa. Boundary layer effects may reduce the evaporation rate by several orders of magnitude. The calculations suggest that limitations on mass transport through the boundary layer may reduce the erosion rate to less than 10  $\mu\text{m/y}$  at wall temperatures up to 2600 K in both Mo and W.

### Section 13.4.1 References:

- [1] J.C. Batty and R. E. Stickney, *J. Chem. Phys.*, Vol. **51**, No. 10 (1969) 4475.
- [2] P. O. Schissel and O. C. Trulson, *J. Chem. Phys.* **43** (1965) 737.
- [3] J. B. Berkowitz-Mattuck, A. Buchler, J. L. Engelke, and S. N. Goldstein, *J. Chem. Phys.* **39** (1963) 2722.
- [4] W. C. Steele, Tech. Rept. AFML-TR-65-343, Pt. II, January 1967, Avo, Wilmington, Mass.
- [5] Y. G. Ptushinskii and B. A. Chuikov, *Surface Sci.*, **6** (1967) 42.
- [6] W. Engelmaier and R. E. Stickney, *Surface Sci.*, **11** (1968) 370.
- [7] W. Geaves and R. E. Stickney, *Surface Sci.*, **11** (1968) 395.
- [8] S. Yamamoto and R. E. Stickney, *Bull. Am. Phys. Soc.*, **14** (1969) 788.

### 13.4.2 Temperature and Oxygen Partial Pressure Limits for V and Ta Alloys

- Oxygen pickup in the Group V metals causes matrix hardening, which in turn produces an increase in the ductile-to-brittle transition temperature (DBTT)
  - (3) oxygen concentration must be below ~1000 ppm to keep Charpy DBTT below room temperature in vanadium (Loomis & Carlson, 1959)
  - (4) the oxygen solubility limit in vanadium is ~1-3 wt.% at T=20-900°C
- All of the Group V metals have high affinity for oxygen; based on thermodynamics alone, extremely low oxygen partial pressures are required to prevent oxygen pickup
  - the vanadium/vanadium oxide solvus occurs at  $10^{-47}$  atm for T=525°C and at  $10^{-36}$  atm at T=725°C (Worrell & Chipman, 1965)

In practice, the matrix oxygen contents can be significantly lower than these thermal equilibrium values due to two effects: 1) Existence of a protective surface oxide film at low temperatures (logarithmic oxide film growth at very low temperatures; parabolic growth at moderate temperatures, >400°C in vanadium); however, linear (rapid) growth occurs at high temperature, and 2) The oxygen impingement flux is strongly reduced at low oxygen partial pressures.

Figure 3: Boundary layer effect model of W and Mo evaporation rates based on 10 MPa He-coolant containing 1 ppm oxygen.

Fig. 13.xx. Effect of interstitial solute additions on the (un-notched) bend transition temperature of vanadium.---Tietz and Wilson (1965), based on data from Loomis and Carlson (1959)

Similar embrittlement behavior has also been observed for V-4Cr-4Ti alloys (e.g., B.A. Pint et al., 1998)

- The kinetics for oxygen pickup in vanadium alloys at moderate to high oxygen partial pressures is controlled by the protective oxide growth rate. However, a high oxygen content (sufficient for embrittlement) exists at depths well beyond the oxide scale layer (Natesan et al. 1998, etc.). The V-4Cr-4Ti activation energy for oxygen diffusion is ~130 kJ/mol (Nakajima et al. 1993, etc.), whereas V-4Cr-4Ti oxide growth has an activation energy of ~180-200 kJ/mol (Uz et al. 1997, etc.). For an exposure time of  $10^4$  h (420 days) at 700°C, the calculated oxide thickness for V-4Cr-4Ti would be only ~0.4 mm (assuming parabolic kinetics) whereas the calculated oxygen diffusion depth would be nearly 4 mm. The corresponding oxygen diffusion depth for exposure at 600°C is 1.6 mm.
- Therefore, the only feasible method to prevent unacceptable oxygen pickup in Group V (vanadium and tantalum) alloys from non-lithium coolants at high temperatures is to limit the oxygen partial pressure. The oxygen impingement flux is  $J_O = P_O(2\pi m_O RT)^{1/2}$ , assuming an equilibration constant of unity. Creation of a monolayer of chemisorbed oxygen on Group V metals at  $T > 400^\circ\text{C}$  requires ~1 Langmuir exposure ( $10^{-6}$  torr-s).
- The following oxygen pressure limits for Group V metals are obtained using the assumptions that subsurface incorporation of the chemisorbed oxygen and matrix oxygen diffusion are not rate-limiting steps (valid for high temperatures and low  $p_O$  levels). Additional assumptions were planar geometry, 3 mm slab thickness, and oxygen ingress from one side only

Oxygen partial pressure	Exposure time to achieve listed oxygen content	
	100 wt.ppm O	1000 wt.ppm O
$10^{-8}$ torr	94 h	940 h
$10^{-10}$ torr	9400 h	94,000 h (11 yr)

In conclusion, oxygen partial pressures below  $10^{-11}$  torr would certainly be sufficient to keep oxygen pickup to acceptably low levels in Group V metals for expected structural material lifetimes (10 to 50 years). Oxygen partial pressures of  $\sim 10^{-10}$  torr may also be tolerable. Boundary layer effects have not been considered in this simple calculation.

### 13.4.3 Review of Corrosion Database for Li, Pb-Li, Sn-Li, and Flibe -coolant Concepts,

Chemical Compatibility of High Temperature Refractory Alloys with Liquid Metals and Flibe (cf. Table 13.x).

- In general, the refractory alloys have very good compatibility with the liquid metals and salts of interest for fusion applications
  - impurity pickup is the key engineering issue
- Li chemical compatibility data base:
  - T-111 (Ta-8W-2Hf) data up to 1370°C (good compatibility; static and circulating loops)
  - Nb-1Zr data up to 1000°C (good compatibility; static and circulating loops)
  - W alloys up to 1370°C (attack observed at  $\geq 1540^\circ\text{C}$ )
  - Mo alloys (TZM) up to 1370°C (attack observed at  $\geq 1540^\circ\text{C}$ )
- Chemical compatibility data base for Flibe  
(generally good compatibility with proposed structural metals)

Table 13.x. Maximum temperatures of structural alloys (bare walls) in contact with high-purity liquid coolants, based on a 5  $\mu\text{m/yr}$  corrosion limit

	Li	Pb-17 Li	Flibe
F/M steel	550-600°C [1,2,3]	450°C [1,2,9]	700°C ? 304/316 st. steel [14]
V alloy	600-700°C [1,4,5]	~650°C [1,10]	?
Nb alloy	>1300°C [6,7]	>600°C [10] (>1000°C in Pb) [11]	>800°C [15]
Ta alloy	>1370°C [6,7]	>600°C [10] (>1000°C in Pb) [11]	?
Mo	>1370°C [6,7]	>600°C [10]	>1100°C? [16,17]
W	>1370°C [6,7]	>600°C [10]	>900°C? [16]
SiC	~550°C ? [8]	>800°C ? [12,13]	?

Table 13.x References:

1. S. Malang and R. Mattas, Fus. Eng. Des. 27 (1995) 399.
2. O.K. Chopra and D.L. Smith, J. Nucl. Mater. 155-157 (1988) 715.
3. P.F. Tortorelli, J. Nucl. Mater. 155-157 (1988) 722.
4. K. Natesan et al., Fus. Eng. Des. 27 (1995) 457.
5. O.K. Chopra and D.L. Smith, J. Nucl. Mater. 155-157 (1988) 683.
6. J.H. Devan et al., Proc. Symp. on Refractory Alloy Technology for Space Nuclear Power Applications, CONF-8308130 (1984) p. 34.
7. J.R. DiStefano, J. Mater. Eng. 11 (1989) 215.
8. D.R. Curran and M.F. Amateau, Am. Ceram. Soc. Bulletin 65, 10 (1986) 1419.
9. M. Broc et al., J. Nucl. Mater. 155-157 (1988) 710.
10. H. Feuerstein et al., J. Nucl. Mater. 233-237 (1996) 1383.
11. H. Shimotake et al., Trans. ANS 10 (1967) 141.

12. P. Hubberstey and T. Sample, J. Nucl. Mater. 248 (1997) 140.
13. J.S. Tulenko and G. Schoessow, Trans. ANS 75 (1996) 72-73
14. J.R. DiStefano, ORNL/TM-12925/R1 (1995).
15. W.D. Manley, Prog. Nucl. Energy, Series IV, 2 (1960) 164.
16. Y. Desai et al., Journal of Metals 40, 7 (1988) A63.
17. J.W. Koger and A.P. Litman, ORNL/TM-2724 (1969).

The limited experimental database on corrosion of structural materials in Sn was reviewed. This information is relevant for the evaluation of Sn and Li as a potential coolant/breeding material in austenitic and ferritic steels which corrode rapidly in Sn at temperature above ~400°C. Additional experimental data are needed for other structural materials, although several materials appear to be compatible with Sn at temperatures of interest for APEX. The physical nature of Sn interaction with structural materials needs to be experimentally examined, so as to plan for corrosion control strategies.

### **Chemical Compatibility of Structural Materials with Molten Tin (static tests)**

- Nb: no corrosion observed at ~600°C  
chemical attack occurred at 800°C [1] and 1000°C [2,3]
- Ta: chemical attack observed at both 600-630 [1,4] and 800°C [1]  
intergranular penetration observed at 1000°C [2,3,5]
- Mo: minimal corrosion observed below ~600°C [4]  
chemical attack observed at both 630 and 800°C [1]  
significant corrosion (predominantly intergranular) observed at 1000°C [2,3-5,6]  
-1.7% weight loss after 340 h at 1000°C [4,6]
- W: good chemical resistance at 630°C; moderate attack at 800°C [1]  
Very little corrosion (10 ppm weight loss) observed after 40 h at 1000°C [6]  
moderate corrosion (<5 µm) observed after 100 h at 1000°C [3]
- Austenitic, Ferritic stainless steels: rapid attack at temperatures above 400-500°C [7]
- SiC: “no interactions detected” for SiC exposed to Sn-Pb-Bi mixture at 760°C [8]

### **Sn corrosion References**

1. J.R. Lance and G.A. Kemeny, Trans. Metall. Soc. AIME and Trans. Quarterly of ASM 56 (1963) 204-205
2. H. Shimotake and J.C. Hesson, Trans. ANS 8 (1965) 413-415
3. H. Shimotake, N.R. Stalica and J.C. Hesson, Trans. ANS 10 (1967) 141-142
4. F.L.LaQue and H.R. Copson, Corrosion Resistance of Metals and Alloys, 2<sup>nd</sup> Ed., ACS Monograph #158 (Reinhold Publ., 1963) 721 pp.
5. T.A. Coultas, MAA-SR-192 (Sept. 15, 1952) 23 pp.
6. E.L. Reed, J. Am. Ceram. Soc. 37 (1954) 146-153

7. Liquid Metals Handbook, 2<sup>nd</sup> ed., Ed. R.N. Lyon, US Office of Naval Research (1952); L.R. Kelman et al., ANL-4417 (1950); ASM Handbook of Corrosion Data, 2<sup>nd</sup> Ed., Eds. B.D. Craig & D.S. Anderson (1992)
8. J.S. Tulenko and G. Schoessow, Trans. ANS 75 (1996) 72-73

### 13.5 Summary and conclusions

- temperature limits (min/max) for evaluated materials and coolants
- additional issues: transmutation, afterheat/safety, availability/proven resources, etc.
- recommended R&D for the next 1 year, next 10 years:
  - chemical compatibility at high T (oxygen, Flibe, Sn-Li including oxidation resistant alloys such as Mo-Ti-Si, intermetallics);
  - unirradiated and irradiated fracture toughness of refractories at high temperatures;
  - joining methods for refractories (stir friction welding , etc.)

Fig. 13.xx

- Lower temperature limit based on radiation hardening/ fracture toughness embrittlement ( $K_{IC} < 30 \text{ MPa}\cdot\text{m}^{1/2}$ ) – large uncertainty for W due to lack of data
- Upper temperature limit based on 100 MPa creep strength (2% in 1000 h); chemical compatibility considerations may cause further decreases in the max operating temp.